# Magnitude and temporal evolution of Dansgaard–Oeschger event 8 abrupt temperature change inferred from nitrogen and argon isotopes in GISP2 ice using a new least-squares inversion

Anais J. Orsi[*], Bruce D. Cornuelle, Jeffrey P. Severinghaus

*Scripps Institution of Oceanography, UCSD, 9500 Gilman Drive, La Jolla, CA 93093-0244, USA*

A B S T R A C T

Polar temperature is often inferred from water isotopes in ice cores. However, non-temperature effects on $\delta^{18}O$ are important during the abrupt events of the last glacial period, such as changes in the seasonality of precipitation, the northward movement of the storm track, and the increase in accumulation. These effects complicate the interpretation of $\delta^{18}O$ as a temperature proxy.

Here, we present an independent surface temperature reconstruction, which allows us to test the relationship between $\delta^{18}O_{ice}$ and temperature, during Dansgaard–Oeschger event 8, 38.2 thousand yrs ago using new $\delta^{15}N$ and $\delta^{40}Ar$ data from the GISP2 ice core in Greenland. This temperature reconstruction relies on a new inversion of inert gas isotope data using generalized least-squares, and includes a robust uncertainty estimation.

We find that both temperature and $\delta^{18}O$ increased in two steps of 20 and 140 yrs, with an overall amplitude of $11.80 \pm 1.8\,°C$ between the stadial and interstadial centennial-mean temperature. The coefficient $\alpha = d\delta^{18}O/dT$ changes with each time-segment, which shows that non-temperature sources of fractionation have a significant contribution to the $\delta^{18}O$ signal. When measured on century-averaged values, we find that $\alpha = d\delta^{18}O/dT = 0.32 \pm 0.06\text{‰}/°C$, which is similar to the glacial/Holocene value of $0.328\text{‰}/°C$.

© 2014 Elsevier B.V. All rights reserved.

## 1. Introduction

### 1.1. Reconstructing polar surface temperature

Temperature is the most fundamental climate variable: as just one example, the equator to pole temperature gradient is the driving force of the general circulation of the atmosphere. When exploring past climates, an accurate temperature history is key to our understanding of atmospheric circulation and the mechanisms of climate change, with relevance to predicting future climate.

Past surface temperature in polar regions is commonly inferred from measured water stable isotopes in ice cores (Dahl-Jensen and Johnsen, 1986; Johnsen et al., 1995; Cuffey and Clow, 1997). The isotopes of oxygen and hydrogen in precipitation fractionate in a complex fashion, in response to the source temperature, the atmospheric pathway, and the condensation temperature at the ice core site (Dansgaard, 1954; Jouzel et al., 1997). In polar re-

gions, the condensation temperature is the dominant source of interannual variability in $\delta^{18}O$ of snow, and, with proper calibration, $\delta^{18}O_{ice}$ can be used to reconstruct the atmospheric temperature (e.g. Dansgaard, 1964; Johnsen et al., 1995, 2001; Jouzel et al., 1997; Stenni et al., 2010; Masson-Delmotte et al., 2008; Masson-Delmotte et al., 2011; Vinther et al., 2009; Buiron et al., 2012). The current spatial variability in $\delta^{18}O_{ice}$ is well correlated with the surface temperature, but this "spatial" calibration is not consistent with temporal variations in $\delta^{18}O_{ice}$ and temperature. As a result, $\delta^{18}O_{ice}$ is generally calibrated using an independent measure of temperature, usually a borehole temperature record (e.g. Johnsen et al., 1995; Cuffey and Clow, 1997).

Borehole temperature profiles provide an absolute estimate of long term surface temperature changes (e.g. Johnsen, 1977; Dahl-Jensen et al., 1998, 1999; Salamatin et al., 1998; Cuffey and Clow, 1997), but cannot resolve high frequency variability. Fast temperature changes can however be inferred from the isotopes of inert gases trapped in ice cores (Severinghaus et al., 1998; Severinghaus and Brook, 1999; Lang et al., 1999; Landais et al., 2004b). This method relies on the diffusion of gases through the firn layer (firn refers to snow older than a year). A sudden change in temperature creates a temperature gradient through the firn,

* Corresponding author st: IPSL/LSCE, CEA/CNRS, l'Orme des merisiers, 91191 Gif s/Yvette, France.
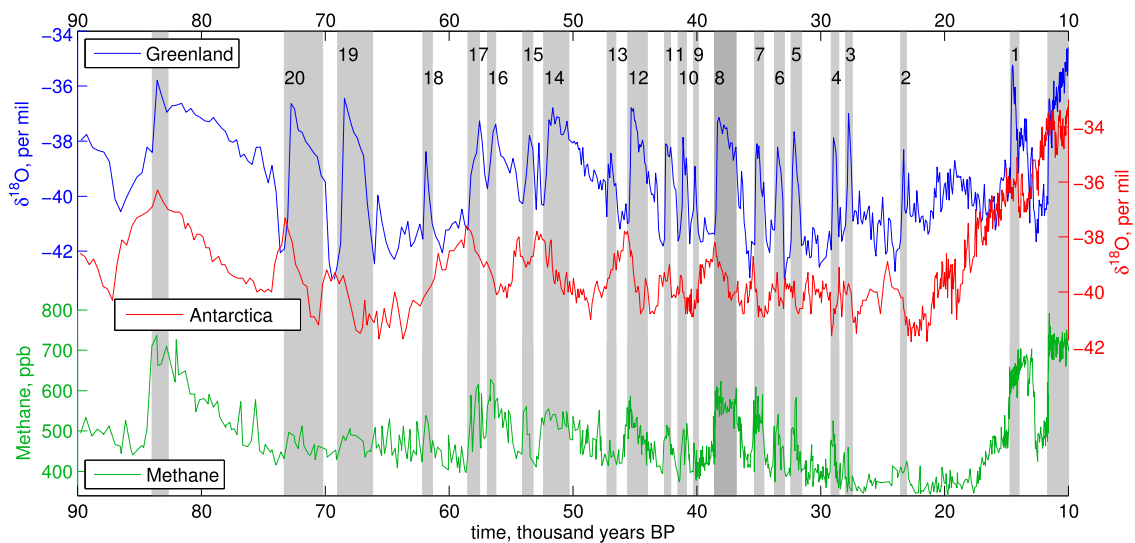*E-mail address:* aorsi@lsce.ipsl.fr (A.J. Orsi).

**Fig. 1.** Overview of polar climate history of the last glacial period, showing measured $\delta^{18}$O in the GISP2 ice core (Greenland; blue), and in the Byrd ice core (Antarctica; red), and a composite atmospheric methane history (green) (Blunier and Brook, 2001). The gray shading highlight the DO events, which are numbered. $\delta^{18}$O is a proxy generally representing temperature. When Greenland experiences an abrupt warming, Antarctica starts a cooling trend. The abrupt warming in Greenland is associated with a sharp increase in methane. (For interpretation of the references to color in this figure legend, the reader is referred to the web version of this article.)

which causes isotopes to fractionate, heavy isotopes concentrating on the colder side. The isotopic composition of inert gases like $N_2$ and Ar does not change significantly in the atmosphere for millions of years (Mariotti, 1983; Sowers et al., 1989), and the changes in $\delta^{15}$N and $\delta^{40}$Ar in the ice core record can be interpreted in terms of temperature change using a temperature diffusion model (Severinghaus et al., 1998; Severinghaus and Brook, 1999). This method is particularly adapted to the study of abrupt climate changes during the last glacial period in Greenland (Lang et al., 1999; Landais et al., 2004a, 2004b; Grachev and Severinghaus, 2005; Huber et al., 2006; Landais et al., 2006b; Capron et al., 2010; Guillevic et al., 2013).

### 1.2. Abrupt climate changes

The last glacial cycle was characterized by a sequence of abrupt climate changes known as Dansgaard–Oeschger (DO) events, happening roughly every 1500 yrs. They were first noticed in water isotope records from Greenland ice cores, as an abrupt warming of 8 to 16 °C in just a few decades, followed by a gradual cooling, and ~1000 yrs later, a rapid cooling back to the cold conditions (Dansgaard et al., 1984, 1993; Alley et al., 1993; Taylor et al., 1993; Severinghaus et al., 1998; Severinghaus and Brook, 1999; Lang et al., 1999; Landais et al., 2004a, 2004b; Grachev and Severinghaus, 2005; Huber et al., 2006; Landais et al., 2006b; Capron et al., 2010). The cold episodes are called stadials, and the warmer episodes interstadials. The term "DO event" refers to the abrupt warming between a stadial and an interstadial. They are numbered from the most recent one to the oldest one (Fig. 1).

The paleoclimate record shows that the abrupt warming in Greenland was associated with large scale circulation changes (Volker and workshop participants, 2002). The storm tracks shifted northwards, and the source of precipitation in Greenland migrated towards colder source water (Sanchez-Goni et al., 2009), which led to an increase in $\delta^{18}$O$_{ice}$. In addition, the snow accumulation increased by 1.5 to 3 times the stadial value (Huber et al., 2006; Thomas et al., 2009; Andersen et al., 2006; Guillevic et al., 2013), partly due to an increase in winter precipitation, which would contribute to a decrease in mean-annual $\delta^{18}$O$_{ice}$ (Masson-Delmotte et al., 2005; Guillevic et al., 2013). All of these factors influenc-

ing the isotopic composition of precipitation are correlated, and there is not enough independent data to isolate the various contributions to changes in $\delta^{18}$O$_{ice}$. As a result, previous studies have assumed that source water, accumulation and precipitation seasonality changes are all directly proportional to temperature, and that $\delta^{18}$O$_{ice}$ can be linearly related to temperature ($\delta^{18}$O$_{ice} = \alpha T + \beta$). The coefficient $\alpha$ has to be adjusted for each event, and varies between 0.29 and 0.55 ‰/°C (Capron et al., 2010, for a review) which is not entirely satisfying, because it has limited predictive skill. In addition, a detailed study of Dansgaard–Oeschger event 8 by Thomas et al. (2009) shows that changes in the circulation preceded changes in Greenland temperature, and several modeling studies have challenged the assumption that local temperature is the dominant contribution to changes in $\delta^{18}$O$_{ice}$ during abrupt changes (e.g. Charles et al., 1994; Tindall and Valdes, 2011).

In this paper, we want to step away from the assumption that $\delta^{18}$O$_{ice}$ is directly proportional to temperature, and analyze inert gas isotope data in a quantitative manner to establish what is actually known about the temperature history during DO events. Previous work using $\delta^{15}$N as a temperature proxy assumed an ideal shape of the temperature history, often a step function (Severinghaus et al., 1998; Severinghaus and Brook, 1999; Grachev, 2004), a slope (Landais et al., 2006a), or relied on a scaling of $\delta^{18}$O (Lang et al., 1999; Leuenberger et al., 1999; Landais et al., 2004a, 2006b; Huber et al., 2006; Kobashi et al., 2007; Capron et al., 2010), which allowed them to reduce the degrees of freedom to just one or two parameters.

Here, we present a temperature reconstruction from a new inverse method applied on new $\delta^{15}$N and $\delta^{40}$Ar data from the GISP-2 ice core during DO-8. Based on generalized least-squares, our inversion does not require specific assumptions regarding the shape of abrupt temperature changes. This technique allows us to clearly separate the unknowns that are constrained by the data from those that are unconstrained (and thus contribute to the uncertainty). We are also able to test the sensitivity to poorly known variables and produce a robust uncertainty estimate. Our reconstruction is a completely independent temperature history at the site, and it can then be used to calibrate $\delta^{18}$O$_{ice}$ on timescales not resolved by borehole temperature.

## 2. Methods

### 2.1. Laboratory measurements

The $\delta^{15}N$ and $\delta^{40}Ar$ samples are taken from the GISP2 ice core, near the summit of Greenland (72.6°N, 38.5°W), covering 24 discrete depths, between 2236.15 m and 2249.85 m, which corresponds to 37.91 to 38.42 ka BP (before 1950 C.E.). Two to 6 samples were run at each depth for $N_2$ (10 g samples) and Ar (50 g samples) isotopes. Nitrogen isotopes were analyzed following the melt/refreeze procedure of Sowers et al. (1989). Argon samples were exposed to a Zr/Al SAES getter at 900 °C to remove $N_2$, $O_2$ and other reactive gases, according to Severinghaus et al. (2003). All samples were run on a MAT 252 mass spectrometer at Scripps Institution of Oceanography. A total of 66 discrete $\delta^{15}N$ measurements were made in January and February 2000, with a pooled standard deviation of 6.4 per meg. A second set of 30 samples was measured in November 2001, but these samples were systematically lower in $\delta^{15}N$, possibly due to a calibration error or storage problem, and were rejected. Argon isotopes were measured in April and May 2001 in duplicates, and the pooled standard deviation of 48 $\delta^{40}Ar$ samples is 13 per meg. Raw measurements were corrected for pressure imbalance and chemical interference in the mass spectrometer, and for gas loss (Severinghaus et al., 2003; Grachev, 2004). The $\delta$-values are calibrated against modern air taken in La Jolla, CA.

### 2.2. Timescale

*Ice timescale*. The official timescale of the GISP2 ice core is from Meese et al. (1997). Since then, a large effort has been made to improve on all Greenland deep ice core timescales, and provide a new layer-counted timescale, called GICC05 (Rasmussen et al., 2006; Andersen et al., 2006; Svensson et al., 2008). This timescale is based on the analysis of many parameters exhibiting a clear annual cycle, measured continuously on the Dye3, GRIP and NGRIP ice cores back to 60 ka BP. The GISP2 core was matched to NGRIP using mainly volcanic tie-points (Rasmussen et al., 2008, I. Seierstad, personal communication, 2013). In the vicinity of DO-8, the maximum counting error, which can be interpreted as a $2\sigma$ error estimate is 1439 yrs, and the relative error between DO-7 and DO-8 is 55 yrs (Andersen et al., 2006). In order to maximize the compatibility with other records, we used the GICC05 age scale for the ice age, and used the Goujon firn densification model (Goujon et al., 2003) to estimate the gas age-ice age difference, $\Delta age$.

*Gas age-ice age difference*. Gases trapped in an ice core do not have the same age as the ice that is surrounding them (Schwander et al., 1988). Atmospheric gases can move readily through the firn and only get locked into the ice at a depth of 70 to 100 m, where the ice is already several hundred years old. The lock-in depth depends on the details of densification of the firn, and changes when the temperature and accumulation rate change (Goujon et al., 2003; Schwander et al., 1997). An increase in temperature will cause the firn to densify faster, and decrease the lock-in-depth, and consequently decrease $\Delta age$ (Herron and Langway, 1980; Goujon et al., 2003; Schwander et al., 1997). An increase in accumulation will have the opposite effect, causing the firn to be thicker, but it will also increase the ice advection, reducing the age of the ice at a certain depth. During a DO event, both the temperature and the accumulation rate increase, and the net effect is a decrease in $\Delta age$.

At the beginning of the transition, the $\Delta age$ is $1066 \pm 20$ yrs, and it decreases during the warming event, to about 600 yrs. In order to maximize the internal consistency of our assumptions, $\Delta age$ is estimated separately by the Goujon model for each scenario of temperature and accumulation history. In other words, the age of
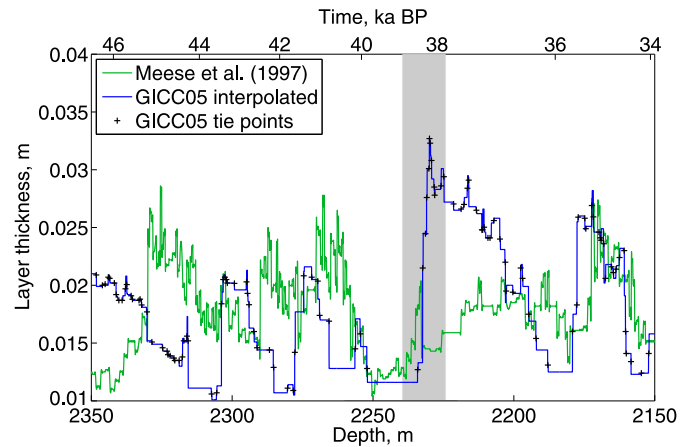


**Fig. 2.** Layer thickness for the Meese et al. (1997) timescale (green), GICC05 linearly interpolated in between tie points (blue). The time is given in thousand years before the year 1950 C.E. The Meese et al. (1997) timescale is not accurate in this depth range, and we used the layer interpolated GICC05 timescale in this study (blue curve). (For interpretation of the references to color in this figure legend, the reader is referred to the web version of this article.)

the gases is a parameter that is estimated by the model, along with $\delta^{15}N$ and $\delta^{40}Ar$.

*Comparison with other timescales*. The observed depth of the abrupt transition at DO-8 constitutes a useful tie-point for timescales. We found that the Meese et al. (1997) ice timescale was offset by 206 yrs from GICC05 at the transition. GICC05 places the date of DO-8 at $38.17 \pm 0.72$ ka BP (Andersen et al., 2006). This timing is consistent with radio-isotope dates from the Sofular speleothem record ($38.14 \pm 0.1$ ka BP, Fleitmann et al., 2009).

### 2.3. Accumulation history

The timescale gives us an estimate of the annual layer thickness $\lambda$ (Fig. 2), which is related to the accumulation rate $\lambda_0$. At the depth we are considering here (2235–2250 m), the uncertainties about the history of the size of the ice sheet make it difficult to estimate the thinning function $c = \lambda_0/\lambda$ by a glaciological model (Cuffey and Clow, 1997). However, we are looking at a small section of the core, so we can consider the thinning function $c$ to be constant through DO-8, and use $c$ as a tunable parameter used in the fit to the inert gas isotope data (see Section 3.2).

### 2.4. Analysis of the inert gas isotope data

The top 2 m of the firn is porous enough to allow air to mix convectively, and have a uniform composition. As the depth increases, the mixing due to surface winds dies out, and convection is no longer possible. In this zone, the air composition is affected by molecular diffusion, where isotopes are separated by two processes: gravitational fractionation and thermal fractionation. As the snow gets denser, bubbles close, effectively sealing the deep firn air composition. We analyze the isotopic composition of $N_2$ and Ar in air bubbles, and derive the gravitational and thermal fractionation happening in the firn diffusive zone.

#### 2.4.1. Gravitational fractionation

Gravitational fractionation is proportional to the depth of the diffusive firn column $Z$ and to the mass difference between the isotopes in a pair $\Delta m$ (Craig et al., 1988; Schwander et al., 1988).

$$\delta^{15}N_g \cong \frac{\Delta mg}{RT}Z \qquad (1)$$

$\delta^{15}N_g$ refers to the gravitational component of the measured $\delta^{15}N$, $g$ is the gravitational constant (9.82 m s$^{-2}$), $R$ the gas constant (8.314 J K$^{-1}$ mol$^{-1}$), and $T$ the mean firn temperature in K.

The diffusive column height $Z$ is smaller than the lock-in depth $Z_{LID}$ because the top few meters of snow have convective mixing of the air with the atmosphere, which prevents fractionation by molecular diffusion (Kawamura et al., 2006, 2013). The depth of the convective zone depends on the site, but it is usually less than 5 m for sites with an accumulation above 5 cm/y (compilation by Landais et al., 2006a). We used a constant 2 m convective zone, consistent with modern conditions at GISP2.

### 2.4.2. Thermal fractionation

Thermal fractionation is proportional to the temperature difference between the top and the bottom of the diffusive column $\Delta T$ (Severinghaus et al., 1998; Severinghaus et al., 2003; Grachev and Severinghaus, 2003a, 2003b):

$$\delta^{15}N_T = \Omega_{15}\Delta T + \epsilon \tag{2}$$

$\delta^{15}N_T$ refers to the thermal component of the measured $\delta^{15}N$. The thermal diffusion sensitivity $\Omega_{15}$ is determined precisely by laboratory measurements (Grachev and Severinghaus, 2003b). $\Omega_{15}\Delta T$ represents the fractionation at equilibrium, and the term $\epsilon$ accounts for the disequilibrium. Gas diffusion through the firn takes about a decade, and $\epsilon$ becomes negligible on timescales longer than a few decades (Kobashi et al., 2008).

### 2.4.3. Smoothing of the raw signal

Gas diffusion and progressive bubble closure cause a broadening of the age distribution of the gases, and hence a smoothing of the gas isotope record (Schwander et al., 1993; Spahni et al., 2003). If we were to neglect this effect, it would lead us to underestimate the magnitude of fast changes needed to fit the $\delta^{15}N$ data. The age broadening can be approximated by a log-normal distribution (Eq. (3)) (Köhler et al., 2010, 2011):

$$p(t-m) = \frac{1}{t\sigma\sqrt{2\pi}}\exp\left(-\frac{1}{2}\left(\frac{\ln(t)-\mu}{\sigma}\right)^2\right) \tag{3}$$

with $p$ is the probability density, $t$ the time, $\mu$ and $\sigma$ the mean and standard deviation of $ln(t)$. The mean of the distribution is $m = \exp(\mu + \sigma^2)$. The width of the smoothing function lies between 10 yrs, the width of the age distribution at the lock-in depth, and 100 yrs, which is the amount of time the ice spends in the lock-in zone. It is difficult to establish precisely, because it is very sensitive to the gas diffusivity in the lock-in zone, which is unknown. We used a value of $\exp(\mu) = 50$ yrs for the inversion presented here. The amplitude of the temperature reconstruction is sensitive to the amount of smoothing used (Landais et al., 2004b), and we estimated that the uncertainty in the smoothing function resulted in an uncertainty of 1.5 °C in the stadial-interstadial temperature difference, which is significant (see Supplement for details).

### 2.5. Isolation of the thermal signal

### 2.5.1. Using two pairs of isotopes

The thermal and gravitational fractionation can be separated by using two isotope pairs, and solving the following system for $\Delta T$ and $Z$ (Severinghaus and Brook, 1999; Grachev, 2004; Landais et al., 2004a, 2004b):

$$\begin{cases} \delta^{15}N = 1\dfrac{g}{RT}Z + \Omega_{15}\Delta T \\ \delta^{40}Ar = 4\dfrac{g}{RT}Z + \Omega_{40}\Delta T \end{cases} \tag{4}$$

We can define $\delta^{15}N_{xs}$, which only depends on temperature, and $\delta^{15}N_g$ which isolates the gravitational component (Severinghaus and Brook, 1999):

$$\begin{cases} \delta^{15}N_{xs} = \delta^{15}N - \dfrac{\delta^{40}Ar}{4} = \left(\Omega_{15} - \dfrac{\Omega_{40}}{4}\right)\Delta T \\ \delta^{15}N_g = \dfrac{g}{RT}Z = \delta^{15}N - \dfrac{\Omega_{15}}{\Omega_{15} - \frac{\Omega_{40}}{4}}\delta^{15}N_{xs} \end{cases} \tag{5}$$

The temperature history can be reconstructed by integrating $\delta^{15}N_{xs}$: the surface temperature at the next time step $T_S(t+dt)$ can be deduced from knowing the temperature at the bottom of the firn $T_B(t)$, and the firn temperature gradient $\Delta T(t)$ at the previous time step (Kobashi et al., 2008):

$$T_S(t+dt) = T_B(t) + \Delta T(t). \tag{6}$$

This method is advantageous because it is independent of changes in accumulation, the temperature advection due to changes in accumulation being of second order, and it does not rely on an imperfect firn densification model (Severinghaus and Brook, 1999). However, the precision of the measurements can limit its application: The pooled standard deviation of $\delta^{15}N$ measurements is $\sigma_{15N} = 6.4$ per meg, and for $\delta^{40}Ar$ it is $\sigma_{40Ar} = 13$ per meg. Thus the precision of $\delta^{15}N_{xs}$ is $\sigma_{xs} = \sqrt{\sigma_{15N}^2 + (\sigma_{40Ar}/4)^2} = 7.2$ per meg, which corresponds to 1.5 °C uncertainty in $\Delta T$. On the other hand, if the gravitational fractionation were known well, the $\sigma_{15N} = 6.4$ per meg uncertainty in $\delta^{15}N$ would correspond to an uncertainty of 0.45 °C in $\Delta T$. Results from this method are discussed in Section 3.1.

### 2.5.2. Using a densification model

Alternatively, we can use a densification model to estimate $Z$ (Goujon et al., 2003; Schwander et al., 1997). Densification is mainly controlled by temperature (a warmer firn densifies faster, yielding a smaller Z) and snow accumulation (the more accumulation, the thicker the firn) (Herron and Langway, 1980). We used a coupled densification and heat transport model (Goujon et al., 2003) to determine the evolution of both the firn thickness $Z$, and the temperature difference between the top and the bottom of the diffusive column $\Delta T$. The inputs of the Goujon model are the histories of temperature and accumulation, and a depth-age relationship for the ice core.

We derived the accumulation history ($\lambda_0$) from a scaling of the layer thickness $\lambda$ with a free parameter $c$: $\lambda_0 = c\lambda$, which is determined by matching the correct firn thickness and $\Delta age$ at the beginning of the abrupt warming. The temperature history corresponding to the $\delta^{15}N$ and $\delta^{40}Ar$ data can be found by running an inversion on the Goujon model. Results from this method are discussed in Section 3.3.

## 3. Results

The magnitude of the temperature change was determined by three methods with increasing complexity. Section 3.1 gives a direct estimate of the temperature change, using $\delta^{15}N_{xs}$. Section 3.2 finds the optimum temperature and accumulation histories by scaling $\delta^{18}O_{ice}$, using just three parameters. The third method relaxes the hypothesis that temperature would be a linear function of $\delta^{18}O_{ice}$, and finds an independent temperature history by a formal linearized least-squares inversion (Section 3.3).

### 3.1. First, and simplest, approach with $\delta^{15}N_{xs}$

To first order, the abrupt change in $\delta^{15}N_{xs}$ can give us the magnitude of the abrupt temperature change (Eq. (5))

(Severinghaus and Brook, 1999; Landais et al., 2004a, 2004b; Grachev, 2004; Kobashi et al., 2007). Indeed, abrupt climate changes are so fast that the temperature at the bottom of the firn $T_{LID}$ does not have time to change, and the change in $\delta^{15}N_{xs}$ directly reflects the change in surface temperature $T_{surf}$:

$$\delta^{15}N_{xs}(2) - \delta^{15}N_{xs}(1)$$
$$= \left( \Omega_{15} - \frac{\Omega_{40}}{4} \right) \left[ \left( T_{surf}(2) - T_{LID}(2) \right) - \left( T_{surf}(1) - T_{LID}(1) \right) \right]$$
$$\approx \left( \Omega_{15} - \frac{\Omega_{40}}{4} \right) \left[ T_{surf}(2) - T_{surf}(1) \right] \tag{7}$$

If the temperature change were not instantaneous, then, for an abrupt warming, we would have $T_{LID}(2) > T_{LID}(1)$, and this method under-estimates the actual warming. For a quantitative estimation of this effect, see Landais et al. (2004b).

We calculated the stadial value of $\delta^{15}N_{xs}$ by taking the mean of the 5 oldest samples: $\delta^{15}N_{xs}(1) = -0.0004 \pm 0.002\%_0$, and took the maximum value of $\delta^{15}N_{xs}(2) = 0.0372 \pm 0.0072\%_0$ to calculate the magnitude of the abrupt change. With $\Omega_{15} = 0.0142\%_0/°C$ and $\Omega_{40} = 0.0381\%_0/°C$ at $-50\,°C$ (Grachev and Severinghaus, 2003a, 2003b), we found that $\Delta T_{surf} = 8.1 \pm 1.5\,°C$.

This first approach is appealing because of its simplicity. However we know that $T_{LID}(2)$ is not equal to $T_{LID}(1)$ (Severinghaus and Brook, 1999; Grachev, 2004). Fifty years after the start of an $8\,°C$ step increase in temperature, $T_{LID}$ has already increased by $1\,°C$. This method therefore provides a lower bound estimate of the abrupt warming.

### 3.2. Temperature history constrained by water isotopes

Alternatively, we can use a densification and heat diffusion model, which computes the thermal and gravitational fractionation from input time series of temperature and accumulation (Schwander et al., 1997; Goujon et al., 2003). We used the Goujon et al. (2003) model (hereafter the Goujon model) which has been widely used for this purpose, and describe the temperature history as a function of $\delta^{18}O$ and the accumulation as a scaling of the annual layer thickness.

The temperature history is described by two parameters $a$ and $b$ such that $T = (\delta^{18}O + b)/a$. The accumulation history is described as a function of the annual layer thickness $\lambda$, with a single parameter $c$: $\lambda_0 = c\lambda$. We found the optimal $a$, $b$ and $c$ using a least-squares fit to the gas isotope data, and using $\Delta age$ at the start of the transition as an additional constraint.

The best fit was found for $a = 0.4027 \pm 0.0026\%_0/°C$, $b = 21.34 \pm 0.12\,°C$ and $c = 4.59 \pm 0.02$ (Fig. 3). The magnitude of the step in $\delta^{18}O$ was estimated by computing the difference between the mean of 150 to 50 yrs before the event, and 100 to 200 yrs after the event. This measure allows us to smooth out the decadal noise in the data. We find a difference $\Delta(\delta^{18}O) = 3.84 \pm 0.54\%_0$, which corresponds to $\Delta T = 9.54 \pm 1.4\,°C$.

### 3.3. Third approach: using an inverse method with fewer assumptions

The relationship between $\delta^{18}O$ and temperature is more complex than a simple linear fit (see Section 1.2). In this section, we wish to relax the assumption that the temperature would scale like $\delta^{18}O$, and explore all the possible histories that would fit $\delta^{15}N$ and $\delta^{40}Ar$ data. This approach allows us to understand more clearly what the constraints on abrupt temperature changes are. To that effect, we linearize the Goujon model, and use a least-squares inverse method to find the optimal solution.
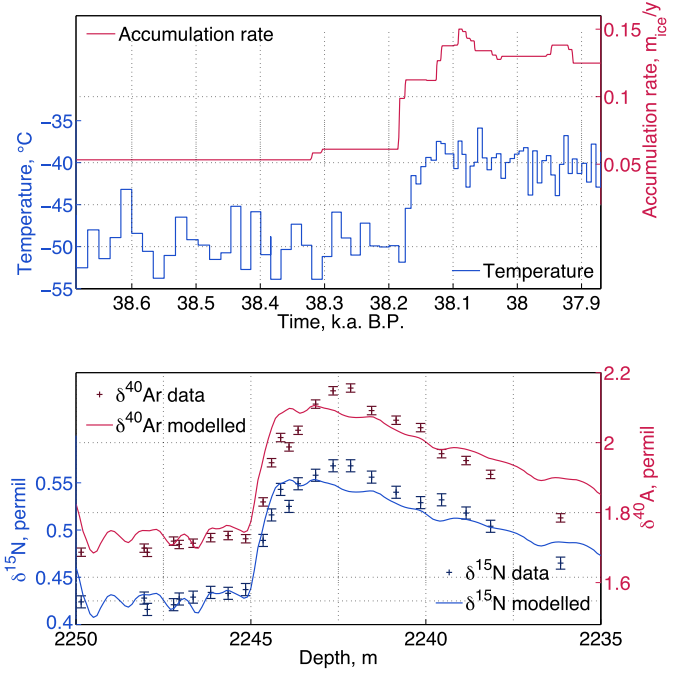


**Fig. 3.** Optimization of the temperature and accumulation histories to match the $\delta^{15}N$ and $\delta^{40}Ar$ data. TOP: Optimal input histories. The accumulation is a scaling of the layer thickness, and the temperature a linear scaling of $\delta^{18}O$. BOTTOM: The fit to $\delta^{40}Ar$ (red) and $\delta^{15}N$ (blue) data. (For interpretation of the references to color in this figure legend, the reader is referred to the web version of this article.)

#### 3.3.1. Linearization of the forward model

The functional space of temperature history can be expressed as a reference guess $T_0$ plus a linear combination of basis functions $b_i(t)$ (see Section 3.3.5 for the choice of basis functions) (Tarantola, 2005, Chapter 6.4):

$$T(t) = T_0(t) + \sum_i x_i b_i(t) \tag{8}$$

where $T(t)$ is a history of temperature, $t$ is the time, and $x_i$ the coefficients of this linear combination. We also introduce a constraint on the accumulation rate $\dot{b}$: $\dot{b} = x_\lambda \lambda$, with $x_\lambda$ a free parameter, and $\lambda$ the annual layer thickness. After discretization, in vectorial notation, Eq. (8) becomes:

$$\begin{bmatrix} \mathbf{T} \\ \dot{b} \end{bmatrix} = \begin{bmatrix} \mathbf{T_0} \\ \dot{b_0} \end{bmatrix} + \mathbf{Bx} \quad \text{with } \mathbf{B} = [\, \mathbf{b}_1 \quad \mathbf{b}_2 \quad \dots \quad \mathbf{b}_n \quad \lambda \,] \tag{9}$$

Discretized equations use bold lower case letters to designate vectors, and bold upper case letters to designate matrices, with the exception of $\mathbf{T}$, which represents the vector of temperature with time.

Each basis $b_i(t)$ was added to $T_0(t)$ and run through the forward model to produce $\delta^{15}N$, $\delta^{40}Ar$ and $\Delta age$ values, $y_i(z)$. We define $h_i(z) = y_i(z) - y_0(z)$, with $y_0$ the output using our initial guess $T_0(t)$. If the model is approximately linear, any $\delta^{15}N$ profile $y(z)$ can be expressed as $y_0$ plus a linear combination of the vectors $h_i(z)$, and a residual $r$:

$$\mathbf{y} = \mathbf{y}_0 + \mathbf{Hx} + \mathbf{r} \quad \text{with } \mathbf{H} = [\, \mathbf{h}_1 \quad \mathbf{h}_2 \quad \dots \quad \mathbf{h}_n \quad \mathbf{h}_\lambda \,] \tag{10}$$

The matrix $\mathbf{H}$ is the linearized and discretized version of the forward model, expressed in the space described by $\mathbf{B}$. It effectively depends on $\mathbf{T}$, or $\mathbf{x}$. For the first iteration, $\mathbf{H} = \mathbf{H}(\mathbf{x}_0)$ with $\mathbf{x}_0 = 0$. All of the model physics is contained in the matrix $\mathbf{H}$, which can be considered as a "black box" from that point on. The validity of using $\mathbf{H}$ as an accurate description of the forward model relies on the linearity of the model around the initial guess $T_0$, thus it is
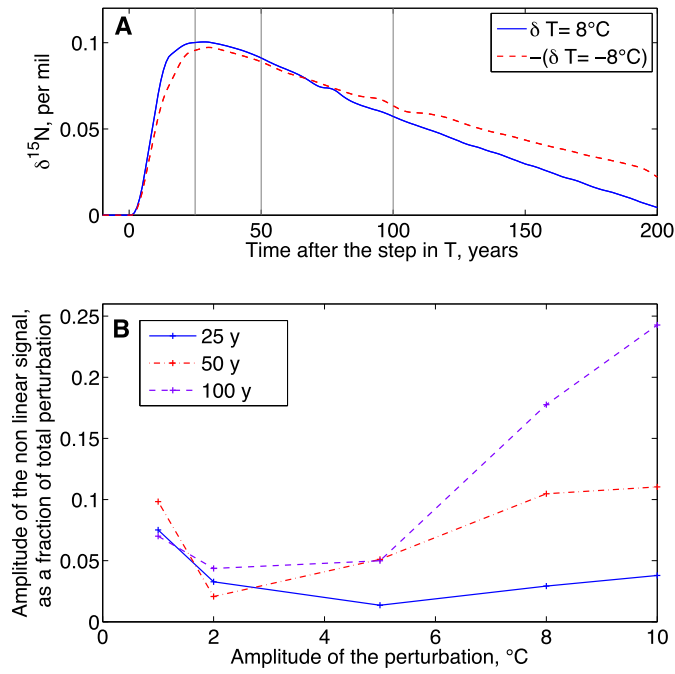
**Fig. 4.** TOP: Output of the Goujon model for a step change in temperature of $8\,^\circ C$, and $-8\,^\circ C$. The perturbation $(\mathbf{y}(\mathbf{x}_0 + \delta\mathbf{x}) - \mathbf{y}(\mathbf{x}_0))$ is plotted in blue, and the opposite perturbation $(\mathbf{y}(\mathbf{x}_0) - \mathbf{y}(\mathbf{x}_0 - \delta\mathbf{x}))$ plotted in red. The mismatch between the two curves is due to non-linearities. BOTTOM: Estimation of the magnitude of the non-linear component of the model, shown as $(\mathbf{r}_{nl}(\delta\mathbf{x}) + \mathbf{r}_{nl}(-\delta\mathbf{x}))/(\mathbf{y}(\mathbf{x}_0 + \delta\mathbf{x}) - \mathbf{y}(\mathbf{x}_0 - \delta\mathbf{x}))$, calculated at 25, 50 and 100 yrs. Non-linearities increase with the amplitude of the perturbation, but remain below 10% of the linear change, which allows us to iterate with a linearized model. (For interpretation of the references to color in this figure legend, the reader is referred to the web version of this article.)

important that $T_0$ would be reasonably close to the true history, as for any linearization problem.

We want to find a history of temperature $T(t)$ that would fit our data $d(z)$. This is equivalent to finding $\mathbf{x}$ so that

$$\mathbf{d} - \mathbf{y}_0 = \mathbf{H}\mathbf{x} + \mathbf{r} \qquad (11)$$

with $\mathbf{r}$ and $\mathbf{x}$ as small as possible, and consistent with their uncertainties.

### 3.3.2. Linearity of the model

The heat advection–diffusion equation is not simply linear, because many parameters, including diffusivity, depend on temperature.

We tested the linearity of the Goujon model, by looking at the size of the non-linear residual $\mathbf{r}$. Eq. (10) can be expanded to:

$$\mathbf{y}(\mathbf{x}_0 + \delta\mathbf{x}) = \mathbf{y}_0 + \mathbf{H}(\mathbf{x}_0)\delta\mathbf{x} + O\left(|\delta\mathbf{x}|^2\right) \qquad (12)$$

Where $\delta\mathbf{x} = \mathbf{x} - \mathbf{x}_0$ is a small perturbation, and $O(|\delta\mathbf{x}|^2)$ represents the higher order terms.

The non-linear residual, $\mathbf{r}_{nl}(\delta\mathbf{x}) = \mathbf{y}(\mathbf{x}_0 + \delta\mathbf{x}) - \mathbf{y}(\mathbf{x}_0) - \mathbf{H}(\mathbf{x}_0)\delta\mathbf{x}$, can be estimated by looking at the difference between opposite perturbations $\delta\mathbf{x}$ and $-\delta\mathbf{x}$. Fig. 4A shows an example of such a perturbation, when we choose for $\delta\mathbf{x}$ a step function of $8\,^\circ C$. The mismatch between the two curves reflects the non-linearities. Fig. 4B shows the magnitude of non-linear perturbation, $(\mathbf{r}_{nl}(\delta\mathbf{x}) + \mathbf{r}_{nl}(-\delta\mathbf{x}))/(\mathbf{y}(\mathbf{x}_0 + \delta\mathbf{x}) - \mathbf{y}(\mathbf{x}_0 - \delta\mathbf{x}))$, as a function of the amplitude of the perturbation $\delta\mathbf{x}$. As expected, the non-linearities increase as the perturbation gets larger, but they are weak enough in the range of temperatures we are considering to allow us to use a linearized model to reconstruct the temperature history (Fig. 4B). Indeed, after the first iteration, $\delta\mathbf{x}$ will be on the order of $1\,^\circ C$ or less, where the model is very linear, which will allow a rapid convergence towards the optimum solution.

### 3.3.3. Inverse model

Diffusion smears out the details of the temperature history, which causes the problem to be under-determined: there are many possible temperature histories that would match the data within uncertainty.

We handle the large number of unknowns by a least square inversion performed on the linearized forward model. This method allows us to identify the undetermined dimensions of the problem, and understand the true uncertainty in the reconstruction.

We solved Eq. (11) by least-squares optimization, minimizing the quadratic cost function

$$\mathcal{J} = \frac{1}{2}\mathbf{r}^T\mathbf{R}^{-1}\mathbf{r} + \frac{1}{2}\mathbf{x}^T\mathbf{P}^{-1}\mathbf{x} \qquad (13)$$

where $\mathbf{P}$ is the inverse of the penalty weighting for model structure, which provides regularization, and $\mathbf{R}$ is the inverse of the penalty weighting for model-data misfit (residuals) $\mathbf{r}$. In a Bayesian framework assuming Gaussian statistics, $\mathcal{J}$ is the negative of the log of the *a-posteriori* likelihood function, where $\mathbf{P}$ is the *a-priori* covariance of uncertainty in the model parameters $\mathbf{x}$, and $\mathbf{R}$ the covariance of uncertainty in the residuals $\mathbf{r}$ (Tarantola and Valette, 1982; Wunsch, 1996).

$\mathbf{P}$ allows us to control the smoothness of the temperature history. We used a set of piecewise linear functions as basis functions $\mathbf{b_i}$, and added a cross correlation between functions. The decorrelation scale was set to 300 yrs before the abrupt warming, 40 years during the abrupt warming, and 100 yrs after the warming. $\mathbf{P}$ was scaled so that the *a-priori* root mean square error was set to $\sigma_x = 5\,^\circ C$.

$\mathbf{R}$ represents not only the error in the data, but also the fact that the model may not be a perfect representation of reality, and may not be expected to fit the data perfectly. We assumed the uncertainty in the residuals to be uncorrelated in time, with time-independent variance, and used a signal to noise ratio of 500, to set the noise level as a function of the signal. The least-squares inversion is not sensitive to the magnitude of $\mathbf{P}$ or $\mathbf{R}$, but to the ratio between them, so it is useful to define $\mathbf{R}$ in terms of signal to noise ratio.

The least-squares theory shows that the optimum solution to (11) is (Wunsch, 1996, Chapter 3):

$$\mathbf{x}_1 = \mathbf{P}\mathbf{H}_1^T\left(\mathbf{H}_1\mathbf{P}\mathbf{H}_1^T + \mathbf{R}\right)^{-1}(\mathbf{d} - \mathbf{y}_o) \qquad (14)$$

The same linearization exercise can be performed around $T_1 = T_0 + \mathbf{B}\mathbf{x}_1$, with the output profile $\mathbf{y}_1$, creating a matrix $\mathbf{H}_2$. Subsequent solutions take the form (El Akkraoui et al., 2008):

$$\sum_{j=1}^{n}\mathbf{x}_j = \mathbf{P}\mathbf{H}_n^T\left(\mathbf{H}_n\mathbf{P}\mathbf{H}_n^T + \mathbf{R}\right)^{-1}\left(\mathbf{d} - \mathbf{y}_{n-1} + \mathbf{H}_n\sum_{j=1}^{n-1}\mathbf{x}_j\right) \qquad (15)$$

The additional term $\mathbf{H}_n\sum_{j=1}^{n-1}\mathbf{x}_j$ is there to keep a consistent constraint on $T_0(t)$. Without it, subsequent iterations could drift away from $T_0(t)$. The history of temperature is recovered using Eq. (9).

### 3.3.4. Uncertainty estimation

The least-squares optimization provides an estimate of the covariance $\hat{\mathbf{P}}$ of the uncertainty in the estimated model parameters:

$$\hat{\mathbf{P}} = \mathbf{P} - \mathbf{P}\mathbf{H}_n^T\left(\mathbf{H}_n\mathbf{P}\mathbf{H}_n^T + \mathbf{R}\right)^{-1}\mathbf{H}_n\mathbf{P} \qquad (16)$$

The eigenvectors of $\hat{\mathbf{P}}$ with the largest eigenvalues represent the dimensions least constrained by the data, which allows us to explore the statistics of the reconstruction. The $1 - \sigma$ error on the reconstruction is given by the square root of the diagonal elements of $\mathbf{S} = \mathbf{B}\hat{\mathbf{P}}\mathbf{B}^T$, but this metric neglects the covariance between the

temperature at a certain time, and the temperature a few years before or after.

An ensemble of solutions to (11) can be created using the eigenvalue decomposition of $\hat{\mathbf{P}} = \mathbf{U}\mathbf{D}\mathbf{U}^T$. The $j$th trial solution $x_j$ takes the form:

$$\mathbf{x}_j = \mathbf{x} + \mathbf{U}\sqrt{\mathbf{D}}\,\mathbf{m}_j \tag{17}$$

with $\mathbf{m}_j$ a vector of Gaussian, independent and identically distributed random numbers with zero mean and unit variance, $\mathbf{x}$ the optimum least-squares solution, and $\sqrt{\mathbf{D}}$ the element by element square root of the diagonal matrix $\mathbf{D}$.

We created a set of 1000 solutions to the least-squares problem using Eq. (17). These solutions allow us to explore the range of possibilities allowed by both the uncertainty in the data, and the unconstrained dimension of the problem. We used these series of solutions to compute the uncertainty in the temperature change.

### 3.3.5. Influence of the parameters used in the inversion

We performed the inversion independently with two set of basis functions: Fourier series and piecewise linear functions. These two sets of basis functions represent two extremes in the representation of the functional space of temperature history: smooth and non-local, or non-smooth and local. Both sets of basis functions were normalized so each element had a maximum amplitude of 1 °C.

The inversion was run on a time window of 2000 yrs, and the mean sampling rate was 27 yrs. To avoid enforcing periodicity, the Fourier components were evenly-spaced harmonics of a 4000 yr fundamental period, extending up to 20 year period. The Fourier components were assumed to be uncorrelated and were given an assumed prior variance proportional to the square of their period. $\mathbf{P}$ was scaled so that the *a-priori* root mean square error was set to $\sigma_x = 5$ °C.

The piece-wise linear components had a spacing of 20 yrs. $\mathbf{P}$ was given the same scaling of $\sigma_x = 5$ °C, but a cross correlation was added: the decorrelation scale was set to 300 yrs before the abrupt warming, 40 yrs during the abrupt warming, and 100 yrs after the warming.

The decorrelation scale is uniform in time for the Fourier series, and it decreases at the time of the abrupt changes for the piecewise linear functions. As a result, the "Fourier" output is somewhat smoother during the abrupt temperature jump, and fits the data less closely (Fig. 5). Aside from the steepest increase, both solutions are very similar, and in particular, they produce the same overall amplitude for the event. We also performed the inversion with piecewise linear functions at a 10-yr resolution (red curve in Fig. 5), and found a temperature reconstruction very similar to that at 20-yr resolution. All three temperature reconstruction fit within the $1 - \sigma$ error computed in Section 3.3.4.

Overall, the temperature reconstructions is only weakly sensitive to the set of basis functions used, or to a reasonable choice of the prior $\mathbf{P}$.

For computational reasons, we present in the following only results with piecewise linear functions at a 20-yr resolution.

### 3.3.6. Inversion results

The inverse method was run to produce a temperature history, as well as the scaling of the annual layer thickness, with the goal to match $\delta^{15}$N, $\delta^{40}$Ar and $\Delta age$ at the beginning of the transition. The results are shown in Fig. 6.

We found that the temperature increased in two steps: the temperature increased by $9.4 \pm 1.6$ °C in the first 20 yrs, followed by a slower increase to a maximum of $12.64 \pm 0.98$ °C after 120 yrs. This temperature history corresponds well with the shape of the $\delta^{18}$O$_{ice}$ curve. We measured the overall amplitude of the event
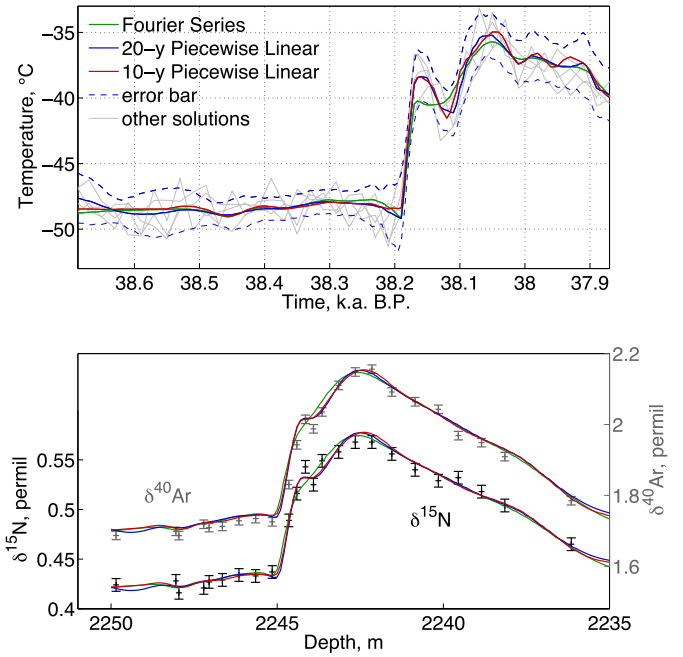


**Fig. 5.** TOP: Surface temperature reconstruction, with different sets of basis functions used in the linearized inversion. Fourier series (in green) are smooth and non-local, and piecewise linear functions with 20 year (blue), and 10 year resolution (red) are non-smooth and localized in time. All yield a very similar reconstruction, showing that the basis on which we linearize the model does not significantly affect the result. BOTTOM: $\delta^{40}$Ar and $\delta^{15}$N profiles corresponding to these histories, and the data. (For interpretation of the references to color in this figure legend, the reader is referred to the web version of this article.)

by taking the mean temperature 150 to 50 yrs before the abrupt warming, and 100 to 200 yrs after the abrupt warming so as to average over decadal variability. We found the amplitude of the event to be $11.80 \pm 0.58$ °C, using a 50-yr log-normal smoothing function. The error bars stated in this section were calculated from the spread of 1000 solutions to the inverse problem, following the method described in Section 3.3.4. The uncertainty in the 100-yr average is lower than at a single point in time, because long term averages are better constrained by the data. We made a detailed assessment of all sources of uncertainty, and found the overall uncertainty in the temperature change to be 1.8 °C (see Supplement).

We estimate the accumulation rate to increase from 0.053 m$_{ice}$/yr to 0.11 m$_{ice}$/yr in 130 yrs followed by an increase to a maximum of 0.15 m$_{ice}$/yr after an additional 100 yrs, although the temporal resolution of the layer thickness is limited. The gas age-ice age difference $\Delta age$ decreased from 1066 yrs to 600 yrs during the interstadial. These values are an improvement over the published Bender et al. (1994) gas–age scale, which was obtained from the synchronization of GISP2 to Vostok using $\delta^{18}$O$_{atm}$.

## 4. Discussion

### 4.1. Accumulation history

The knowledge of both the firn thickness and $\Delta age$ before the abrupt change allows us to find the value of the thinning function, and derive the accumulation rate from the depth-age scale. We find that $\lambda_0/\lambda = 4.59 \pm 0.045$, for a stadial accumulation rate of 0.053 m$_{ice}$/yr. This value is somewhat model dependent. Different densification models produce different firn thicknesses for the same temperature and accumulation pair, and we have found that the Goujon model needs to be 2 °C colder than the Herron and Langway (1980) model to get the same firn thickness. In addition,
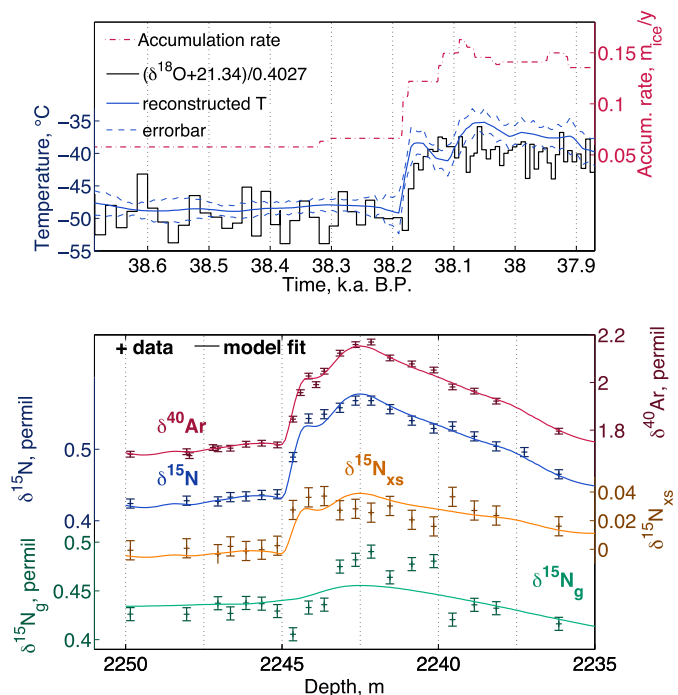
**Fig. 6.** Surface temperature reconstruction. TOP: Accumulation rate derived from annual layer thickness (red), and surface temperature reconstruction, with an initial guess of 10 °C step change (blue); the black line shows the temperature history based on $\delta^{18}O_{ice}$. BOTTOM: from top to bottom: $\delta^{40}Ar$ (red), $\delta^{15}N$ (blue), $\delta^{15}N_{xs}$ (brown) and $\delta^{15}N_g$ (green) data (symbols), and model fit (line). (For interpretation of the references to color in this figure legend, the reader is referred to the web version of this article.)

the presence of a convective zone can mislead our estimation of the firn thickness from inert gas isotopes.

Regardless of the absolute value, the annual layer thickness itself suggests a tripling of the accumulation rate at GISP2 during the abrupt warming. This estimation is compatible with the changes in the gravitational fractionation seen in the $\delta^{15}N$ data, and is unlikely to be merely an artifact of a change in the deformation of the ice between dusty, ductile, stadial ice and clean, hard, interstadial ice. We tested for that by allowing an additional offset in the accumulation history using $\lambda_0 = c\lambda + d$ but the model found the optimum value of $d$ to be zero.

The increase in the accumulation rate is larger at GISP2 than at NGRIP (50% increase, Thomas et al., 2009), or at NEEM (Guillevic et al., 2013). This evidence supports the idea that a decrease in sea ice in the Nordic sea is responsible for a large increase in precipitation in the southern part of Greenland during DO events, but that its impact on northern Greenland is more limited (Li et al., 2010).

### 4.2. Temperature history and water isotopes

Although there are some notable differences between $\delta^{18}O_{ice}$ and the least-squares temperature reconstruction, the general shape of the event is similar, and we find that the inert gas isotope data support the idea that variations in $\delta^{18}O_{ice}$ are dominated by local temperature changes.

The abrupt increase into Interstadial 8 took place in two steps: First, a sharp increase of 4.15‰ and 9.4 °C in the first 20 yrs, followed by a slower increase to maximum of +6.43‰ and 12.64 °C after 120 yrs.

We can compare $\delta^{18}O_{ice}$ with our new temperature reconstruction, and evaluate $\alpha = d\delta^{18}O/dT$ for both the fast and slow part of the warming (Table 1).

**Table 1**
Calculation of $\alpha = d\delta^{18}O/dT$ at different time during DO8.

| Time ka BP | d($\delta^{18}O$) (‰) | dT (°C) | $\alpha$ (‰/°C) |
|---|---|---|---|
| 38.180–38.170 | 4.15 | 9.37 | 0.443 |
| 38.230–38.040 | 6.40 | 12.64 | 0.506 |
| $\delta$ (100-yr mean) | 3.84 | 11.80 | 0.325 |

We find that $\alpha$ is larger for fast changes than for the century average. The 100-yr mean $\alpha$ is similar to the glacial/Holocene value of 0.328‰/°C (Cuffey and Clow, 1997). During cold stadials, winter precipitation is largely suppressed (Werner et al., 2000), but during the abrupt warming, winter precipitation resumes, which causes a decrease in $\delta^{18}O$ (Masson-Delmotte et al., 2005). We find that $\alpha$ is smaller during the abrupt warming than during the subsequent more gradual temperature increase, which suggests that the impact of precipitation seasonality might be more prevalent at the very beginning of the DO event than later on. The lack of a plateau between 38.170 and 38.111 ka BP in $\delta^{18}O$, and the generally poor fit to the data during the second part of the temperature increase (Fig. 3) indicates that there are significant non-temperature contributions to the $\delta^{18}O$ signal.

### 4.3. Future improvements

The dominant source of uncertainty in the temperature reconstruction from inert gas isotopes is the unknown smoothing due to progressive bubble closure. Ice cores from the same location can have different diffusivities and age distributions in the lock-in zone (Buizert et al., 2012), and it is unlikely that lock-in zone parameters may be accurately derived from bulk properties. The width of the smoothing function could be estimated from independent knowledge of the timing of the increase in $CH_4$ during a DO event, from a higher accumulation site, and comparison to the gas profile of the core of interest.

Densification models cannot reproduce the fine structure of the variations in $\delta^{15}N_{grav}$. Most current models rely on the parameterization of bulk density and porosity (e.g. Herron and Langway, 1980; Goujon et al., 2003), but the fine structure, especially the density variability, may be very important for the estimation of the depth at which gravitational fractionation ceases (Hörhold et al., 2009; Hörhold et al., 2011; Freitag et al., 2013). Future models, based on a layered firn, and incorporating grain growth in the densification equations (Arthern et al., 2010) are likely to improve the estimation of the lock-in depth, and help interpret the inert gas isotopic signal.

### 5. Conclusions

We have presented a new method to reconstruct the surface temperature history from inert gas isotopes in ice cores. The temperature increase at Dansgaard Oeschger event 8 had an amplitude of 11.80 ± 1.8 °C over a period of 140 yrs. The dominant source of uncertainty is due to the unknown smoothing due to diffusion and progressive bubble closure in the lock-in zone, which is estimated conservatively to be ±1.5 °C, and the overall uncertainty is $\sigma = 1.8$ °C (see Supplement for details). Both temperature and $\delta^{18}O_{ice}$ exhibit a warming in two phases, suggesting that $\delta^{18}O$ is linearly correlated with local temperature changes to first order. However, we find different $\alpha = d\delta^{18}O/dT$ for different segments, which indicates that changes in precipitation seasonality are more prevalent near the very beginning of DO8. In addition, the mismatch between 38.170 and 38.040 ka BP reminds us that sources of fractionation other than temperature have a significant contribution to the $\delta^{18}O$ signal. The century average $\alpha = 0.325 \pm 0.06$‰/°C

is very similar to the glacial/Holocene value of 0.328 (Cuffey and Clow, 1997).

Inert gas isotopes also contain information regarding past firn thickness. We used this information to derive the magnitude of the thinning of annual layers in the vicinity of DO8, 38.2 ka BP, at 2245 m depth. We found that $\lambda_0/\lambda = 4.59 \pm 0.04$. This value can help constrain models of ice sheet evolution (Cuffey and Clow, 1997).

The development of this technique, measured concurrently with all water isotopes, will allow us to disentangle the sources of fractionation of water isotopes, improve the precision of our temperature estimation and enhance our understanding of the relationship between water isotopes and climate.

## Acknowledgements

## Appendix A. Supplementary material

Supplementary material related to this article can be found online at http://dx.doi.org/10.1016/j.epsl.2014.03.030.

## References

Alley, R., Meese, D., Shuman, C., Gow, A., Taylor, K., Grootes, P., White, J., Ram, M., Waddington, E., Mayewski, P., Zielinski, G., 1993. Abrupt increase in Greenland snow accumulation at the end of the Younger Dryas event. Nature 362, 527–529.

Andersen, K., Svensson, A., Johnsen, S., Rasmussen, S., Bigler, M., Röthlisberger, R., Ruth, U., Siggaard-Andersen, M., Peder Steffensen, J., Dahl-Jensen, D., Vinther, B.M., Clausen, H.B., 2006. The Greenland ice core chronology 2005, 15–42 ka. Part 1: constructing the time scale. Quat. Sci. Rev. 25, 3246–3257.

Arthern, R.J., Vaughan, D.G., Rankin, A.M., Mulvaney, R., Thomas, E.R., 2010. In situ measurements of Antarctic snow compaction compared with predictions of models. J. Geophys. Res., Earth Surf. 115.

Bender, M., Sowers, T., Dickson, M., Orchardo, J., Grootes, P., Mayewski, P., Meese, D., 1994. Climate correlations between Greenland and Antarctica during the past 100,000 years. Nature 372, 663–666.

Blunier, T., Brook, E.J., 2001. Timing of millennial-scale climate change in Antarctica and Greenland during the last glacial period. Science 291, 109–112.

Buiron, D., Stenni, B., Chappellaz, J., Landais, A., Baumgartner, M., Bonazza, M., Capron, E., Frezzotti, M., Kageyama, M., Lemieux-Dudon, B., Masson-Delmotte, V., Parrenin, F., Schilt, A., Selmo, E., Severi, M., Swingedouw, D., Udisti, R., 2012. Regional imprints of millennial variability during the MIS 3 period around Antarctica. Quat. Sci. Rev. 48, 99–112.

Buizert, C., Martinerie, P., Petrenko, V.V., Severinghaus, J.P., Trudinger, C.M., Witrant, E., Rosen, J.L., Orsi, A.J., Rubino, M., Etheridge, D.M., Steele, L.P., Hogan, C., Laube, J.C., Sturges, W.T., Levchenko, V.A., Smith, A.M., Levin, I., Conway, T.J., Dlugokencky, E.J., Lang, P.M., Kawamura, K., Jenk, T.M., White, J.W.C., Sowers, T., Schwander, J., Blunier, T., 2012. Gas transport in firn: multiple-tracer characterisation and model intercomparison for NEEM, Northern Greenland Gas transport in firn: multiple-tracer characterisation and model intercomparison for NEEM, Northern Greenland. Atmos. Chem. Phys. 12, 4259–4277.

Capron, E., Landais, A., Chappellaz, J., Schilt, A., Buiron, D., Dahl-Jensen, D., Johnsen, S., Jouzel, J., Lemieux-Dudon, B., Loulergue, L., Leuenberger, M., Masson-Delmotte, V., Meyer, H., Oerter, H., Stenni, B., 2010. Millennial and sub-millennial scale climatic variations recorded in polar ice cores over the last glacial period. Clim. Past 6, 345–365.

Charles, C.D., Rind, D., Jouzel, J., Koster, R.D., Fairbanks, R.G., 1994. Glacial-interglacial changes in moisture sources for Greenland: influences on the ice core record of climate. Science 263, 508–511.

Craig, H., Horibe, Y., Sowers, T., 1988. Gravitational separation of gases and isotopes in polar ice caps. Science 242, 1675–1678.

Cuffey, K., Clow, G., 1997. Temperature, accumulation, and ice sheet elevation in central Greenland through the last deglacial transition. J. Geophys. Res. 102, 26238–26296.

Dahl-Jensen, D., Johnsen, S., 1986. Palaeotemperatures still exist in the Greenland ice sheet. Nature 320, 250–252.

Dahl-Jensen, D., Morgan, V.I., Elcheikh, A., 1999. Monte carlo inverse modelling of the Law Dome (Antarctica) temperature profile. Ann. Glaciol. 29 (6), 145–150.

Dahl-Jensen, D., Mosegaard, K., Gundestrup, N., Clow, G.D., Johnsen, S.J., Hansen, A.W., Balling, N., 1998. Past temperatures directly from the Greenland ice sheet. Science 282, 268–271.

Dansgaard, W., 1954. The O18-abundance in fresh water. Geochim. Cosmochim. Acta 6, 241–260.

Dansgaard, W., 1964. Stable isotopes in precipitation. Tellus 16, 436–468.

Dansgaard, W., Johnsen, S., Clausen, H., Dahl-Jensen, D., Gundestrup, N., Hammer, C., Hvidberg, C., Steffensen, J., Sveinbjörnsdottir, A., Jouzel, J., Bond, G., 1993. Evidence for general instability of past climate from a 250-kyr ice-core record. Nature 364, 218–220.

Dansgaard, W., Johnsen, S., Clausen, H., Dahl-Jensen, D., Gundestrup, N., Hammer, C., Oeschger, H., 1984. North Atlantic climatic oscillations revealed by deep Greenland ice cores. Clim. Process. Clim. Sensitiv. 29, 288–298.

El Akkraoui, A., Gauthier, P., Pellerin, S., Buis, S., 2008. Intercomparison of the primal and dual formulations of variational data assimilation. Q. J. R. Meteorol. Soc. 134, 1015–1025.

Fleitmann, D., Cheng, H., Badertscher, S., Edwards, R., Mudelsee, M., Göktürk, O., Fankhauser, A., Pickering, R., Raible, C., Matter, A., Kramers, J., Tüysüz, O., 2009. Timing and climatic impact of Greenland interstadials recorded in stalagmites from northern Turkey. Geophys. Res. Lett. 36, L19707.

Freitag, J., Kipfstuhl, S., Laepple, T., Wilhelms, F., 2013. Impurity-controlled densification: a new model for stratified polar firn. J. Glaciol. 59, 1163–1169.

Goujon, C., Barnola, J., Ritz, C., 2003. Modeling the densification of polar firn including heat diffusion: application to close-off characteristics and gas isotopic fractionation for Antarctica and Greenland sites. J. Geophys. Res., Atmos. 108, 4792.

Grachev, A., Severinghaus, J., 2003a. Determining the thermal diffusion factor for $^{40}Ar/^{36}Ar$ in air to aid paleoreconstruction of abrupt climate change. J. Phys. Chem. A, Mol. Spectrosc. Kinet. Environ. Gen. Theory 107, 4636–4642.

Grachev, A., Severinghaus, J., 2003b. Laboratory determination of thermal diffusion constants for $^{29}N_2/^{28}N_2$ in air at temperatures from $-60$ to $0\,^\circ C$ for reconstruction of magnitudes of abrupt climate changes using the ice core fossil-air paleothermometer. Geochim. Cosmochim. Acta 67, 345–360.

Grachev, A.M., 2004. Laboratory-determined air thermal diffusion constants applied to reconstructing the magnitudes of past abrupt temperature changes from gas isotope observations in polar ice cores. PhD thesis. University of California, San Diego.

Grachev, A.M., Severinghaus, J.P., 2005. A revised $+10 \pm 4$ C magnitude of the abrupt change in Greenland temperature at the Younger Dryas termination using published GISP2 gas isotope data and air thermal diffusion constants. Quat. Sci. Rev. 24, 513–519.

Guillevic, M., Bazin, L., Landais, A., Kindler, P., Orsi, A., Masson-Delmotte, V., Blunier, T., Buchardt, S., Capron, E., Leuenberger, M., et al., 2013. Spatial gradients of temperature, accumulation and $\delta^{18}O$-ice in Greenland over a series of Dansgaard–Oeschger events. Clim. Past 9, 1029–1051.

Herron, M.M., Langway, C.C. Jr., 1980. Firn densification, an empirical model. J. Glaciol. 25, 373–386.

Hörhold, M.W., Albert, M.R., Freitag, J., 2009. The impact of accumulation rate on anisotropy and air permeability of polar firn at a high-accumulation site. J. Glaciol. 55, 625–630.

Hörhold, M.W., Kipfstuhl, S., Wilhelms, F., Freitag, J., Frenzel, A., 2011. The densification of layered polar firn. J. Geophys. Res. 116.

Huber, C., Leuenberger, M., Spahni, R., Flückiger, J., Schwander, J., Stocker, T.F., Johnsen, S., Landais, A., Jouzel, J., 2006. Isotope calibrated Greenland temperature record over Marine Isotope Stage 3 and its relation to $CH_4$. Earth Planet. Sci. Lett. 243, 504–519.

Johnsen, S., 1977. Stable isotope profiles compared with temperature profiles in firn with historical temperature records. Int. Assoc. Hydrolog. Sci. Publ. 118, 388–392.

Johnsen, S., Dahl-Jensen, D., Dansgaard, W., Gundestrup, N., 1995. Greenland palaeotemperatures derived from GRIP bore hole temperature and ice core isotope profiles. Tellus B 47, 624–629.

Johnsen, S., Dahl-Jensen, D., Gundestrup, N., Steffensen, J., Clausen, H.B., Miller, H., Masson-Delmotte, V., Sveinbjornsdottir, A., White, J.W., 2001. Oxygen isotope and palaeotemperature records from six Greenland ice-core stations: Camp Century, Dye-3, GRIP, GISP2, Renland and NorthGRIP. J. Q. Sci. 16, 299–307.

Jouzel, J., Alley, R., Cuffey, K., Dansgaard, W., Grootes, P., Hoffmann, G., Johnsen, S., Koster, R., Peel, D., Shuman, C., Stievenard, M., Stuiver, M., White, J., 1997. Validity of the temperature reconstruction from water isotopes in ice cores. J. Geophys. Res. 102, 26.

Kawamura, K., Severinghaus, J.P., Albert, M.R., Courville, Z.R., Fahnestock, M.A., Scambos, T., Shields, E., Shuman, C.A., 2013. Kinetic fractionation of gases by deep air convection in polar firn. Atmos. Chem. Phys. 13, 11141–11155.

Kawamura, K., Severinghaus, J.P., Ishidoya, S., Sugawara, S., Hashida, G., Motoyama, H., Fujii, Y., Aoki, S., Nakazawa, T., 2006. Convective mixing of air in firn at four polar sites. Earth Planet. Sci. Lett. 244, 672–682.

Kobashi, T., Severinghaus, J.P., Barnola, J.M., 2008. $4 \pm 1.5$ C abrupt warming 11,270 years ago identified from trapped air in Greenland ice. Earth Planet. Sci. Lett. 268, 397–407.

Kobashi, T., Severinghaus, J.P., Brook, E.J., Barnola, J.M., Grachev, A.M., 2007. Precise timing and characterization of abrupt climate change 8200 years ago from air trapped in polar ice. Quat. Sci. Rev. 26, 12112–12222.

Köhler, P., Fischer, H., Schmitt, J., 2010. Atmospheric $\delta^{13}CO_2$ and its relation to $pCO_2$ and deep ocean $\delta^{13}C$ during the late pleistocene. Paleoceanography 25.

Köhler, P., Knorr, G., Buiron, D., Lourantou, A., Chappellaz, J., 2011. Abrupt rise in atmospheric $CO_2$ at the onset of the Bølling/Allerød: in-situ ice core data versus true atmospheric signals. Clim. Past 7, 473–486.

Landais, A., Barnola, J., Kawamura, K., Caillon, N., Delmotte, M., Van Ommen, T., Dreyfus, G., Jouzel, J., Masson-Delmotte, V., Minster, B., Freitag, J., Leuenberger, M., Schwander, J., Huber, C., Etheridge, D., Morgan, V., 2006a. Firn-air $\delta^{15}N$ in modern polar sites and glacial-interglacial ice: a model-data mismatch during glacial periods in Antarctica?. Quat. Sci. Rev. 25, 49–62.

Landais, A., Barnola, J.M., Masson-Delmotte, V., Jouzel, J., Chappellaz, J., Caillon, N., Huber, C., Leuenberger, M., Johnsen, S.J., 2004a. A continuous record of temperature evolution over a sequence of Dansgaard–Oeschger events during Marine Isotopic Stage 4 (76 to 62 kyr BP). Geophys. Res. Lett. 31.

Landais, A., Caillon, N., Goujon, C., Grachev, A., Barnola, J., Chappellaz, J., Jouzel, J., Masson-Delmotte, V., Leuenberger, M., 2004b. Quantification of rapid temperature change during DO event 12 and phasing with methane inferred from air isotopic measurements. Earth Planet. Sci. Lett. 225, 221–232.

Landais, A., Masson-Delmotte, V., Jouzel, J., Raynaud, D., Johnsen, S., Huber, C., Leuenberger, M., Schwander, J., Minster, B., 2006b. The glacial inception as recorded in the NorthGRIP Greenland ice core: timing, structure and associated abrupt temperature changes. Clim. Dyn. 26, 273–284.

Lang, C., Leuenberger, M., Schwander, J., Johnsen, S., 1999. 16 °C rapid temperature variation in central Greenland 70,000 years ago. Science 286, 934–937.

Leuenberger, M.C., Lang, C., Schwander, J., 1999. Delta $^{15}N$ measurements as a calibration tool for the paleothermometer and gas-ice age differences: a case study for the 8200 BP event on GRIP ice. J. Geophys. Res., Atmos. 1984–2012 (104), 22163–22170.

Li, C., Battisti, D.S., Bitz, C.M., 2010. Can North Atlantic Sea ice anomalies account for Dansgaard–Oeschger climate signals?. J. Climate 23, 5457–5475.

Mariotti, A., 1983. Atmospheric nitrogen is a reliable standard for natural $^{15}N$ abundance measurements. Nature 303, 685–687.

Masson-Delmotte, V., Buiron, D., Ekaykin, A., Frezzotti, M., Gallee, H., Jouzel, J., Krinner, G., Landais, A., Motoyama, H., Oerter, H., Pol, K., Pollard, D., Ritz, C., Schlosser, E., Sime, L.C., Sodemann, H., Stenni, B., Uemura, R., Vimeux, F., 2011. A comparison of the present and last interglacial periods in six Antarctic ice cores. Clim. Past 7, 397–423.

Masson-Delmotte, V., Hou, S., Ekaykin, A., Jouzel, J., Aristarain, A., Bernardo, R., Bromwich, D., Cattani, O., Delmotte, M., Falourd, S., Frezzotti, M., Gallee, H., Genoni, L., Isaksson, E., Landais, A., Helsen, M.M., Hoffmann Lopez, J., Morgan, V., Motoyama, H., Noone, D., Oerter, H., Petit, J.R., Royer, A., Uemura, R., Schmidt, G.A., Schlosser, E., Simões, J.C., Steig, E.J., Stenni, B., Stievenard, M., van den Broeke, M.R., van de Wal, R.S.W., van de Berg, W.J., Vimeux, F., White, J.W.C., 2008. A review of antarctic surface snow isotopic composition: observations, atmospheric circulation, and isotopic modeling*. J. Climate 21, 3359–3387.

Masson-Delmotte, V., Jouzel, J., Landais, A., Stievenard, M., Johnsen, S., White, J., Werner, M., Sveinbjornsdottir, A., Fuhrer, K., 2005. GRIP deuterium excess reveals rapid and orbital-scale changes in Greenland moisture origin. Science 309, 118–121.

Meese, D., Gow, A., Alley, R., Zielinski, G., Grootes, P., Ram, M., Taylor, K., Mayewski, P., Bolzan, J., 1997. The Greenland ice sheet project 2 depth-age scale: methods and results. J. Geophys. Res. 102, 26.

Rasmussen, S., Andersen, K., Svensson, A., Steffensen, J., Vinther, B., Clausen, H., Siggaard-Andersen, M., Johnsen, S., Larsen, L., Dahl-Jensen, D., Bigler, M., Röthlisberger, R., Fischer, H., Goto-Azuma, K., Hansson, M.E., Ruth, U., 2006. A new Greenland ice core chronology for the last glacial termination. J. Geophys. Res. 111, D06102.

Rasmussen, S., Seierstad, I., Andersen, K., Bigler, M., Dahl-Jensen, D., Johnsen, S., 2008. Synchronization of the NGRIP, GRIP, and GISP2 ice cores across MIS 2 and palaeoclimatic implications. Quat. Sci. Rev. 27, 18–28.

Salamatin, A., Lipenkov, V., Barkov, N., Jouzel, J., 1998. Ice core age dating and paleothermometer calibration based on isotope and temperature profiles from deep boreholes at Vostok station (East Antarctica). J. Geophys. Res. 103, 8963–8977.

Sanchez-Goni, M.F., Landais, A., Cacho, I., Duprat, J., Rossignol, L., 2009. Contrasting intrainterstadial climatic evolution between high and middle North Atlantic latitudes: a close-up of Greenland Interstadials 8 and 12. Geochem. Geophys. Geosyst. 10, 1–16.

Schwander, J., Barnola, J., Andrie, C., Leuenberger, M., Ludin, A., Raynaud, D., Stauffer, B., 1993. The age of the air in the firn and the ice at summit, Greenland. J. Geophys. Res. 98, 2831–2838.

Schwander, J., Sowers, T., Barnola, J.M., Blunier, T., Fuchs, A., Malaizé, B., 1997. Age scale of the air in the summit ice: implication for glacial–interglacial temperature change. J. Geophys. Res. 102, 19483–19493.

Schwander, J., Stauffer, B., Sigg, A., 1988. Air mixing in firn and the age of the air at pore close-off. Ann. Glaciol. 10.

Severinghaus, J., Grachev, A., Luz, B., Caillon, N.A., 2003. A method for precise measurement of argon 40/36 and krypton/argon ratios in trapped air in polar ice with applications to past firn thickness and abrupt climate change in Greenland and at Siple Dome, Antarctica. Geochim. Cosmochim. Acta 67, 325–343.

Severinghaus, J.P., Brook, E.J., 1999. Abrupt climate change at the end of the last glacial period inferred from trapped air in polar ice. Science 286, 930–934.

Severinghaus, J.P., Sowers, T., Brook, E.J., Bender, M.L., Alley, R.B., 1998. Timing of abrupt climate change at the end of the Younger Dryas interval from thermally fractionated gases in polar ice. Nature 391, 141–146.

Sowers, T., Bender, M., Raynaud, D., 1989. Elemental and isotopic composition of occluded $O_2$ and $N_2$ in polar ice. J. Geophys. Res. 94, 5137–5150.

Spahni, R., Schwander, J., Flückiger, J., Stauffer, B., Chappellaz, J., Raynaud, D., 2003. The attenuation of fast atmospheric $CH_4$ variations recorded in polar ice cores. Geophys. Res. Lett. 30.

Stenni, B., Masson-Delmotte, V., Selmo, E., Oerter, H., Meyer, H., Röthlisberger, R., Jouzel, J., Cattani, O., Falourd, S., Fischer, H., Hoffmann, G., Iacumin, P., Johnsen, S., Minster, B., Udisti, R., 2010. The deuterium excess records of EPICA Dome C and Dronning Maud Land ice cores (East Antarctica). Quat. Sci. Rev. 29, 146–159.

Svensson, A., Andersen, K., Bigler, M., Clausen, H., Dahl-Jensen, D., Davies, S., Johnsen, S., Muscheler, R., Parrenin, F., Rasmussen, S., Röthlisberger, R., Seierstad, I., Steffensen, J.P., Vinther, B.M., 2008. A 60 000 year Greenland stratigraphic ice core chronology. Clim. Past 4, 47–57.

Tarantola, A., 2005. Inverse Problem Theory and Methods for Model Parameter Estimation. Society for Industrial and Applied Mathematics.

Tarantola, A., Valette, B., 1982. Generalized nonlinear inverse problems solved using the least squares criterion. Rev. Geophys. 20, 219–232.

Taylor, K.C., Hammer, C.U., Alley, R.B., Clausen, H.B., Dahl-Jensen, D., Gow, A.J., Gundestrup, N.S., Kipfstuh, J., Moore, J.C., Waddington, E.D., 1993. Electrical conductivity measurements from the GISP2 and GRIP Greenland ice cores. Nature 366, 549–552.

Thomas, E., Wolff, E., Mulvaney, R., Johnsen, S., Steffensen, J., Arrowsmith, C., 2009. Anatomy of a Dansgaard–Oeschger warming transition: high-resolution analysis of the North Greenland ice core project ice core. J. Geophys. Res. 114, D08102.

Tindall, J.C., Valdes, P.J., 2011. Modeling the 8.2 ka event using a coupled atmosphere–ocean gcm. Glob. Planet. Change 79, 312.

Vinther, B.M., Buchardt, S.L., Clausen, H.B., Dahl-Jensen, D., Johnsen, S.J., Fisher, D.A., Koerner, R.M., Raynaud, D., Lipenkov, V.Y., Blunier, T., Rasmussen, S.O., Steffensen, J.P., Svensson, A.M., 2009. Holocene thinning of the Greenland ice sheet. Nature 461, 385–388.

Volker, A., workshop participants, 2002. Global distribution of centennial-scale records for Marine Isotope Stage (MIS) 3: a database. Quat. Sci. Rev. 21, 1185–1212.

Werner, M., Mikolajewicz, U., Heimann, M., Hoffmann, G., 2000. Borehole versus isotope temperatures on Greenland: seasonality does matter. Geophys. Res. Lett. 27, 723–726.

Wunsch, C., 1996. The Ocean Circulation Inverse Problem. Cambridge Univ. Press.